

# CALCULATION OF LONGITUDINAL CSR IMPEDANCE IN CURVED CHAMBER

Demin Zhou<sup>\*A,B)</sup>, Kazuhito Ohmi<sup>B)</sup>, Katsunobu Oide<sup>B)</sup>, Lei Zang<sup>B)</sup>,

<sup>A)</sup>The Graduate University for Advanced Studies[SOKENDAI]  
Shonan Village, Hayama, Kanagawa 240-0193 Japan

<sup>B)</sup>High Energy Accelerator Research Organization, KEK  
1-1 Oho, Tsukuba, Ibaraki 305-0801 Japan

## Abstract

Coherent synchrotron radiation (CSR) fields are generated when a bunched beam moves along a curved trajectory. A new code, named CSRZ, was developed using finite difference method to calculate the longitudinal CSR impedance for a beam moving along a curved chamber. The method adopted in our code was originated by T. Agoh and K. Yokoya [1]. It solves the parabolic equation in the frequency domain in a curvilinear coordinate system. In our studies, the chamber has uniform rectangular cross-section along the beam trajectory, which is the same as that in [1]. But the curvature of the beam trajectory is freed, and then we can investigate the CSR impedance of a single or a series of bending magnets. The calculation results indicate that the shielding effect due to outer chamber wall can be well explained by a simple optical approximation model at high frequencies. With an approximation of a wiggling chamber inside a wiggler, the coherent wiggler radiation (CWR) impedance has also been studied. Due to chamber shielding, the CWR impedance exhibits narrow peaks at frequencies satisfying the resonant conditions.

## INTRODUCTION

CSR generated by an ultra-relativistic beam moving in a toroidal chamber has been studied extensively. The steady-state CSR in free space was addressed in [2, 3]. The transient effect in free space was studied in [4]. The steady-state CSR in a rectangular toroidal chamber was also well understood [5, 6, 7]. The steady-state CSR between parallel plates has been studied in [8].

For a single bending magnet with a vacuum chamber, T. Agoh, G. Stupakov, et al. have developed different methods to calculate the CSR impedance of a single magnet [1, 9]. This paper follows Agoh and Yokoya's method [1] to calculate CSR generated by a beam moving along an arbitrary trajectory. The trajectory can be generated by a single bending magnet (see Fig. 1(a)), a series of bending magnets (extending the chamber of Fig. 1(a) by adding more curved sections), or by a wiggler (or an undulator) (see Fig. 1(b)). At present, we assume the chamber has an uniform rectangular cross-section along the beam trajectory. To close the problem, two long straight sections are added before the

entrance and after the exit of the chamber. We continue the work presented in [1, 9] and do investigations in the follow aspects: 1) the features of longitudinal CSR impedance in a single bending magnet; 2) Optical approximation of CSR; 3) the longitudinal CWR impedance of a wiggler.

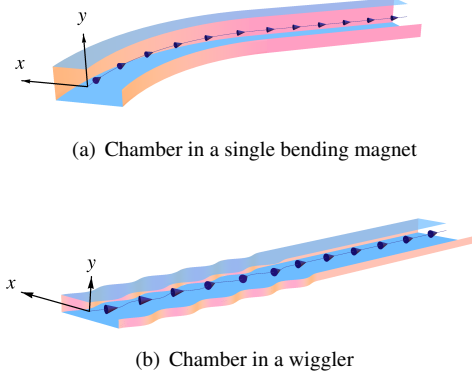


Figure 1: The geometries of the curved chamber for a single bending magnet and a wiggler. A infinitely long straight chamber is connected after the exit of the curved chamber. The beam moves along the curved line with arrows. The origin of the coordinate system coincides with the beam orbit.

## PROBLEM STATEMENT

The fundamental equation adopted in our studies of CSR is the parabolic equation in the frequency domain in a curvilinear coordinate with the origin on the beam trajectory [1, 10]

$$\frac{\partial \vec{E}_\perp}{\partial s} = \frac{i}{2k} \left( \nabla_\perp^2 \vec{E}_\perp - \frac{1}{\epsilon_0} \nabla_\perp \rho_0 + \frac{2k^2 x}{R(s)} \vec{E}_\perp \right), \quad (1)$$

where  $\vec{E}_\perp$  is the transverse electric field, and  $R(s)$  is the  $s$ -dependent bending radius along the beam orbit.  $\epsilon_0$  is the vacuum permittivity. The beam is assumed to be rigid, i.e. the beam charge density  $\rho_0$  does not vary along  $s$ .

With paraxial approximation [1], the longitudinal electric field is a byproduct of the transverse fields and approximated as,

$$E_s = \frac{i}{k} \left( \nabla_\perp \cdot \vec{E}_\perp - \mu_0 c J_s \right), \quad (2)$$

\* dmzhou@post.kek.jp

where  $\mu_0$  is the vacuum permeability,  $c$  is the speed of light in vacuum, and  $J_s = \rho_0 c$  is the current density. The detailed derivation of the above equations can be found in Refs. [10, 1]. We will not discuss the validity of these equations either, because it has been well addressed in Refs. [9, 7].

Equation (1) also describes the field evolution in a straight chamber where the inverse bending radius is zero

$$\frac{\partial \vec{E}_\perp}{\partial s} = \frac{i}{2k} \left( \nabla_\perp^2 \vec{E}_\perp - \frac{1}{\epsilon_0} \nabla_\perp \rho_0 \right). \quad (3)$$

In our calculations, the beam has a point charge form in the longitudinal direction and Gaussian distribution in the transverse directions. Then the longitudinal impedance is calculated by directly integrating  $E_s$  over  $s$

$$Z_{\parallel}(k) = -\frac{1}{q} \int_0^\infty E_s(x_c, y_c) ds \quad (4)$$

where  $(x_c, y_c)$  denotes the center of the beam in the transverse  $x$ - $y$  plane. The appearance of the minus sign in Eq.(4) is due to the convention of the beam instability formalism.

The numerical algorithms adopted in our work are adapted from the mesh methods originally presented in [1]. We start by dividing the rectangular domain  $(0, a) \times (0, b)$  in the  $x$ - $y$  plane into an equidistant  $M \times N$  mesh with step sizes  $\Delta x = a/M$  and  $\Delta y = b/N$  in the  $x$  and  $y$  directions, respectively. The grid is shown in the solid lines of Fig. 2. The numerical techniques will not be discussed in this paper. The readers are referred to [1, 11] for details.

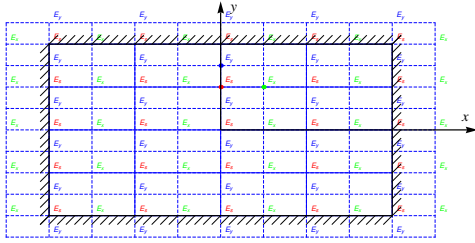


Figure 2: Staggered grid definition with ghost points outside the boundary of the chamber. The positions of various field components are shown. Constant spacing in the  $x$  and  $y$  directions is assumed.

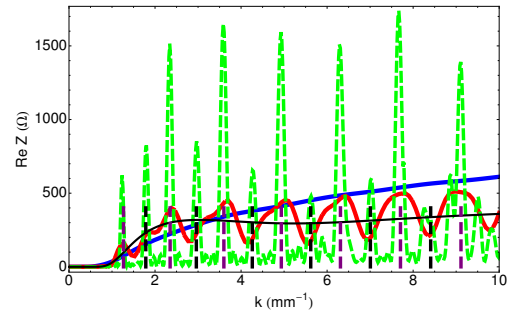
## NUMERICAL RESULTS

In this section, we present a few examples of calculating the longitudinal CSR and CWR impedances. In all these calculations, the beam is assumed to move along the central line of the curved chamber, i.e.  $x_c = a/2, y_c = b/2$ .

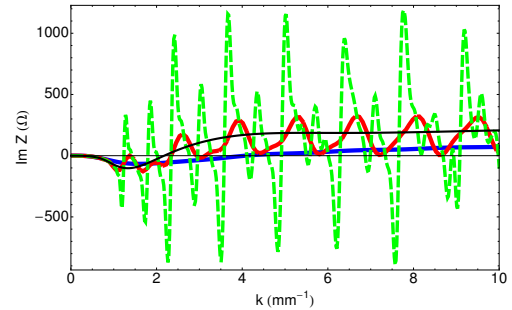
### Single bending magnet

For the first example, we investigate the influence of the magnet length on the longitudinal CSR impedance. We

choose bending radius  $R = 5$  m, chamber cross-section dimensions  $a = 6$  cm,  $b = 3$  cm. The magnet length is varied as  $L_b = 0.5, 2, 8$  m. The impedance results are shown in Fig. 3. In the same figures, we also plot the results given by the parallel plates model in solid black lines [1]. And the corresponding wake potentials with a short bunch of rms length  $\sigma_z = 0.5$  mm are given in Fig. 4. When  $L_b = 0.5$  m, which indicates a short curved chamber, the impedance is very smooth. When the curved chamber gets longer, the impedance becomes fluctuating with an interval of around  $1.3 \text{ mm}^{-1}$  in wavenumber and eventually results in a series of resonant peaks. This observation clearly indicates that the CSR impedance is actually related to the eigenmodes of the curved chamber [10]. When the curved chamber is long enough, some specific modes which fulfill the phase matching condition can be strongly excited by the beam and become dominant in the radiation field.



(a) Real part (The purple and black dashed lines denote  $E_x$  and  $E_y$  modes with  $n = 1$ , respectively.)



(b) Imaginary part

Figure 3: CSR impedance for a single bending magnet with  $R = 5$  m and varied length of the curved chamber  $L_b = 0.5, 2, 8$  m. The dimensions of the chamber cross-section are  $a = 6$  cm, and  $b = 3$  cm. The impedances have been normalized by the length of the curved chamber. Blue solid lines:  $L_b = 0.5$  m; red solid lines:  $L_b = 2$  m; green dashed lines:  $L_b = 8$  m; black solid lines: parallel plates model.

One can compare the wavenumbers at the resonant peaks in Fig. 3(a) with the analytical predictions which are available in Refs. [7, 6, 10]. According to [7], the resonance peaks should appear at wavenumbers of

$$k_{mn} = \frac{n\pi}{b} \sqrt{\frac{R}{x_b}} \Upsilon \left( \frac{b(m \pm 0.25)}{nx_b} \right), \quad (5)$$

where the integer indices  $m$  and  $n$  denote the individual

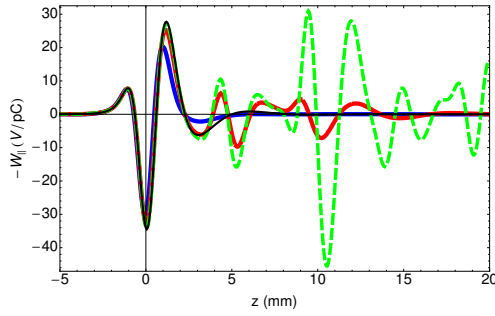


Figure 4: Short-bunch wake potentials due to CSR in a single bending magnet with  $R = 5$  m and varied length of the curved chamber  $L_b = 0.5, 2, 8$  m. The dimensions of the chamber cross-section are  $a = 6$  cm, and  $b = 3$  cm. The gaussian bunch length  $\sigma_z = 0.5$  mm with bunch head to the left side. The wake potentials have been normalized by the length of the curved chamber. Blue solid lines:  $L_b = 0.5$  m; red solid lines:  $L_b = 2$  m; green dashed lines:  $L_b = 8$  m; black solid lines: parallel plates model.

mode of the curved chamber and  $x_b$  is the distance from the beam orbit to the outer wall in the horizontal plane. The plus sign in Eq.(5) indicates  $E_x$  modes in which  $E_y = 0$  and  $m = 0, 1, 2, 3, \dots$ ; the minus sign indicates  $E_y$  modes in which  $E_x = 0$  and  $m = 1, 2, 3, \dots$ . According to [7],  $n$  must be odd and  $n = 1, 3, 5, \dots$ . Finally,  $\Upsilon(r)$  is defined by

$$\Upsilon(r) = \left[ \left( \sqrt{1 + \frac{r^2}{3}} + 1 \right)^{\frac{1}{3}} - \left( \sqrt{1 + \frac{r^2}{3}} - 1 \right)^{\frac{1}{3}} \right]^{-\frac{3}{2}}. \quad (6)$$

When  $r$  is large,  $\Upsilon(r)$  can be approximated by  $3r/2^{3/2}$  [7]. It implies that the resonance peaks in the CSR impedance are almost equally spaced along the wavenumber axis. The resonances are indicated by vertical dashed lines in Fig. 3(a). It turns out that they agree well with the observed peaks from numerical calculations.

As stated in [7, 9], when the aspect ratio of the curved chamber  $a/b$  is larger than 2, the shielding of the side walls can be neglected and the parallel plates model is a good approximation for a long bending magnet. This criteria works well in the low frequency region with  $k < k_{th}$  which was proved in [7]. Here  $k_{th}$  is the shielding threshold defined by [7]

$$k_{th} = \pi \sqrt{\frac{R}{b^3}}. \quad (7)$$

Our calculations do agree with this criteria. On the contrary, in the high frequency region, the CSR impedance may significantly differ from the parallel plates model and exhibit fluctuations and even narrow resonance peaks for a long magnet. A geometrical explanation for this observation was proposed in Ref. [12] as illustrated in Fig. 5. The CSR field is radiated in the direction tangent to the beam trajectory when a beam enters the curved chamber. The outer wall plays a role of mirror and reflects the field back to the beam. If the curved chamber is long enough, the re-

flected field can accumulate and become significant. The geometrical picture of CSR suggests a critical length of

$$L_c = 2R\theta_c \approx 2\sqrt{2Rx_b}, \quad (8)$$

for the bending magnet. Here  $\theta_c = \text{ArcCos}(R/(R+x_b)) \approx \sqrt{2x_b/R}$ . If  $L_b \gg L_c$ , some specific modes can be strongly excited and results in the fluctuations or resonant peaks in the CSR impedance. If  $L \leq L_c$ , such fluctuations will be negligible. But if  $L \ll L_c$ , transient effect will also become important. The critical length indicates a length when the reflection of the outer wall becomes important. But  $L_c$  does not depends on the aspect ratio of the chamber cross-section. Therefore, the condition of neglecting side-wall shielding, i.e.  $L \leq L_c$ , can be a supplement to the criteria of  $a/b \geq 2$  which only applies at low frequency limit, i.e.  $k < k_{th}$ .

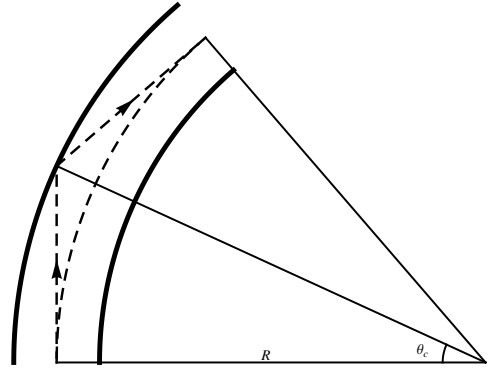


Figure 5: CSR reflected by the outer wall of the beam pipe. The beam starts to radiate fields at the entrance of the curved chamber. The dashed curve without arrows on it denotes the beam orbit. The arrowed dashed lines represent the direction of the radiation fields.

Similar to optical approximation in the theory of geometric impedance [13], the  $L_c$  defined by Eq. (8) can also be interpreted as a catch-up distance over which the CSR, generated by the head of a beam, reflects from the outer wall and reaches the beam tail at length  $\Delta s$  behind the head. It's easy to calculate  $\Delta s$  from the geometry shown in Fig. 5, and the result is [12]

$$\Delta s = 2R(\text{Tan}(\theta_c) - \theta_c) \approx \frac{4}{3} \sqrt{\frac{2x_b^3}{R}}. \quad (9)$$

The quantity  $\Delta s$  corresponds to a modulation frequency of [12]

$$\Delta k = \frac{2\pi}{\Delta s} \approx \frac{3\pi}{2} \sqrt{\frac{R}{2x_b^3}}. \quad (10)$$

It turns out that  $\Delta k = k_{(m+1)n} - k_{mn}$  is exactly the distance between adjacent resonances for the same vertical index  $n$  and large argument  $r$  in Eq.(6). When comparing  $\Delta s$  with the bunch length  $\sigma_z$ , one can find another condition of neglecting outer-wall shielding effect in evaluating CSR induced instability, i.e.  $\Delta s \gg \sigma_z$ . Namely, this condition

says that the reflected CSR fields from the outer wall can never catch up with the beam tail and thus has no influence on the beam in total.

One can check Eqs.(9) and (10) by applying them to the examples depicted in Fig. 3(a).  $\Delta k = 1.4 \text{ mm}^{-1}$  is close to the observed value of  $1.3 \text{ mm}^{-1}$ .  $\Delta s = 4.4 \text{ mm}^{-1}$  is roughly the distance at which the first peak appears in the tail part of the wake potential in Fig. 4. Since the bunch length  $\sigma_z = 0.5 \text{ mm}$  is much smaller than  $\Delta s$ , the amplitude of the wake potential in the vicinity of the beam is almost independent of magnet length. Thus, one can conclude that the outer-wall shielding mainly impose effect in the tail part of CSR wake.

### CWR in a wiggler

Next we present a wiggler example where the oscillations of the beam are confined to the horizontal plane. We assumed the applicable conditions as: wiggler parameter  $K \gg 1$  and  $K/\gamma \ll 1$  where  $\gamma$  is the relativistic factor. The beam traversing through the wiggler undergoes sinusoidal motion, to first-order approximation. Thus the curvature of the beam orbit can be approximated by a cosine function as following:

$$R^{-1}(s) = R_0^{-1} \cos(k_w s), \quad (11)$$

where  $R_0^{-1}$  is the maximum curvature and  $k_w$  is the wavenumber of the wiggler field.

Since we have assumed that the chamber cross-section is uniform along the beam orbit, the chamber inside the wiggler is modeled as a ‘‘wiggling’’ one in our calculations. The effect of a wiggling chamber was well discussed and compared with analytically obtained results in Ref. [14]. It was found that in the case of large aspect ratio, a wiggling chamber is a good approximation. For exemplification of our approach, we set the parameters of a wiggler as: maximum bending radius  $R_0 = 100 \text{ m}$  and magnetic field wavelength  $\lambda_w = 2\pi/k_w = 1 \text{ m}$ , and the number of periods  $N_w = 10$ . The chamber width and height are set to be  $a = 10 \text{ cm}$  and  $b = 2 \text{ cm}$ . The results are shown in Fig. 6. The wake potentials with rms bunch length of  $0.5 \text{ mm}$  corresponding to the impedances are plotted in Fig. 7. It turns out that the CWR with chamber shielding can differ remarkably from the free-space model [15].

By enlarging the chamber height, we can test the shielding effect of up- and down-side chamber walls. This is demonstrated in Figs. 8 and 9. In these calculations, the chamber height is varied as  $b = 2, 5, 10 \text{ cm}$  and all other parameters are kept the same as in the previous example. Both the impedance and wake potential tend to be close to that of free-space model while the chamber height is enlarged.

In [14], the real part impedance in a rectangular chamber

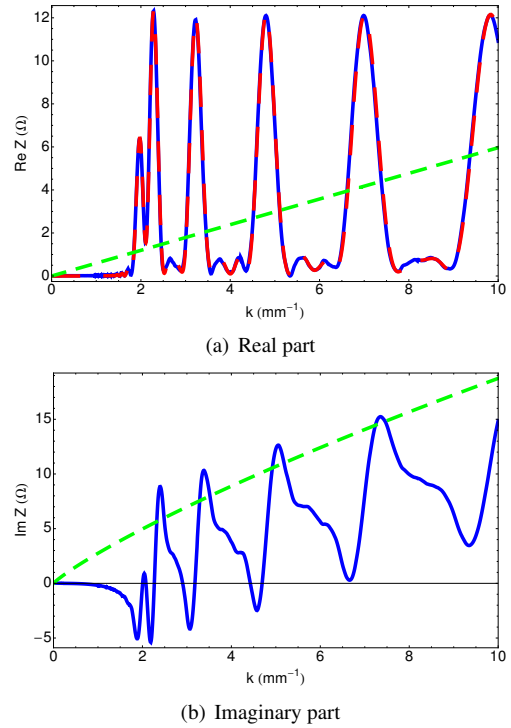


Figure 6: CWR impedance of a wiggler. The blue lines are numerical results. The dashed red line and dashed green lines are given by Eq.(12) and Eq.(15), respectively.

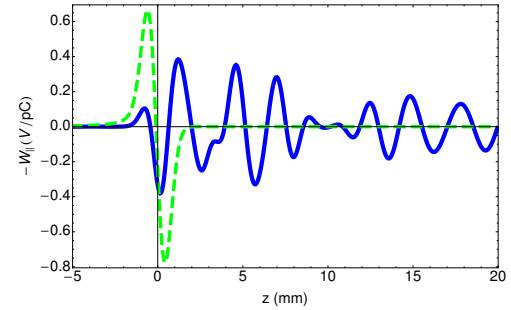


Figure 7: Short-bunch wake potentials due to CWR in a wiggler. The gaussian bunch length  $\sigma_z = 0.5 \text{ mm}$  with bunch head to the left side. Blue solid line: with shielding of vacuum chamber; Green dashed line: free-space model.

was calculated analytically using mode expansion method

$$\text{Re } Z_{\parallel}(k) = \frac{4Z_0}{abR_0^2} \sum_{m=0}^{\infty} \sum_{n=1}^{\infty} \frac{k}{(1 + \delta_{m0})k_z} \frac{\sin^2((k - k_z - k_w)L_w/2)}{(k - k_z)^2 - k_w^2}, \quad (12)$$

where  $k_z = \sqrt{k^2 - \alpha_{mn}^2}$  with  $\alpha_{mn} = \sqrt{k_x^2 + k_y^2}$ ,  $k_x = m\pi/a$  and  $k_y = n\pi/b$ .  $L_w = N_w(2\pi/k_w)$  is the total length of the wiggler. The summation in Eq.(12) goes over the even values of  $m$  and the odd values of  $n$ . Equation (12) also indicates the resonance condition

$$k - k_z - k_w = 0, \quad (13)$$

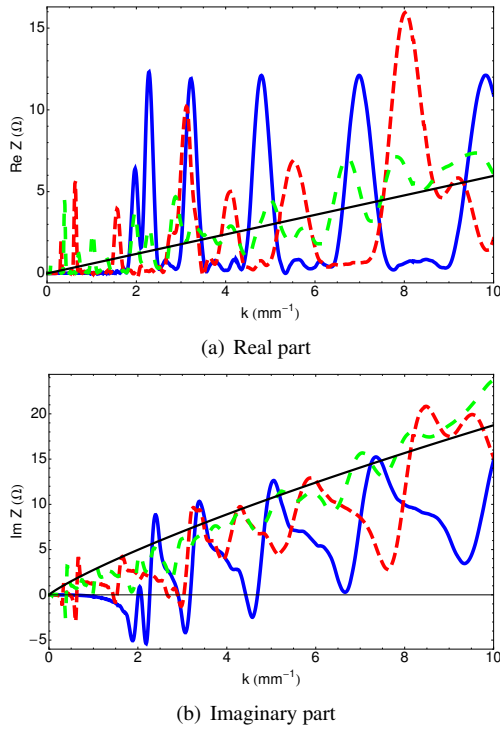


Figure 8: CWR impedance of a wiggler with  $b = 2, 5, 10$  cm. Blue solid lines:  $b = 2$  cm; red dashed lines:  $b = 5$  cm; green dashed lines:  $b = 10$  cm; black solid lines: free-space model.

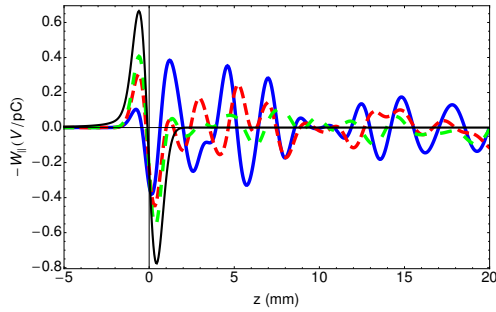


Figure 9: Short-bunch wake potentials due to CWR in a wiggler with  $b = 2, 5, 10$  cm. The gaussian bunch length  $\sigma_z = 0.5$  mm with bunch head to the left side. Blue solid lines:  $b = 2$  cm; red dashed lines:  $b = 5$  cm; green dashed lines:  $b = 10$  cm; black solid lines: free-space model.

which shows that the resonant peaks in impedance should appear at

$$k_{mn} = \frac{\alpha_{mn}^2 + k_w^2}{2k_w}. \quad (14)$$

The resonant peaks in Fig.6(a) do agree with the above equation. The impedance for a wiggler in free space is given in [15]

$$Z_{||}(k) = \frac{1}{4} Z_0 L_w k \frac{k_w}{k_0} \left( 1 - \frac{2i}{\pi} \left( \log \frac{4k}{k_0} + \gamma_E \right) \right), \quad (15)$$

where  $k_0 = 4k_w^3 R_0^2$  is the fundamental radiation wavenumber with wiggler parameter  $K \gg 1$  and  $\gamma_E \approx 0.577$  is the

Euler constant. One sees that the numerical results again agree well with the analytic formula Eq.(12) but disagree with Eq.(15). Specially, the imaginary part does not show the property of linear slope in the limit of low frequency which is predicted by the free space model.

## SUMMARY

In this paper we presented the numerical calculations of the longitudinal CSR impedance for a beam moving in an arbitrarily curved chamber. The CSRZ code was used to investigate the properties of CSR impedance of a single bending magnet. It turns out that the magnet length, in addition to the chamber aspect ratio, may also play an important role in defining the structure of CSR impedance. For a long magnet, the shielding effect of the outer wall can be well understood using an optical approximation model. CWR of a wiggler was also studied with a tiny approximation in modeling the vacuum chamber. With shielding of the chamber considered, the CWR impedance and wake potential of a wiggler might be quite different from the free-space model. This observation agree with an independent analytic approach.

The author D.Z. would like to thank K. Yokoya, T. Agoh, G. Stupakov and Y.H. Chin for valuable discussions.

## REFERENCES

- [1] T. Agoh and K. Yokoya, Phys. Rev. ST Accel. Beams, 7(5):054403 (2004).
- [2] B. G. Schinov, A. G. Bonch-Osmolovski, V. G. Makhankov and V. N. Tsytovitch, Plasma Physics 15 (1973) 211.
- [3] A. Faltens and L. J. Laslett, Part. Accel. 4, 151. (1973).
- [4] E. L. Saldin, E. A. Schneidmiller and M. V. Yurkov, Nucl. Instrum. Methods A, 490:1-8, 2002.
- [5] K.-Y. Ng, Part. Accel. 25, 153. (1990).
- [6] R. L. Warnock and P. Morton, Part. Accel. 25, 113. (1990).
- [7] T. Agoh, Phys. Rev. ST Accel. Beams, 12(9):094402 (2009).
- [8] J. B. Murphy, S. Krinsky and R. L. Gluckstern, Part. Accel. 57, 9. (1997).
- [9] G. V. Stupakov and I. A. Kotelnikov, Phys. Rev. ST Accel. Beams, 12(10):104401 (2009).
- [10] G. V. Stupakov and I. A. Kotelnikov, Phys. Rev. ST Accel. Beams, 6(3):034401 (2003).
- [11] D. Zhou, PhD thesis, KEK/SOKENDAI, 2011.
- [12] K. Oide, Talk at CSR mini-workshop, KEK, Nov. 8, 2010.
- [13] G. V. Stupakov, K. L. F. Bane and I. Zagorodnov, Phys. Rev. ST Accel. Beams, 10(5):054401 (2007).
- [14] G. V. Stupakov and D. Zhou, KEK Preprint 2010-43, KEK, Tsukuba, 2010.
- [15] J. Wu, O. Raubenheimer, and G. V. Stupakov, Phys. Rev. ST Accel. Beams, 6(4):040701 (2003).